

PCCP

Accepted Manuscript



This is an *Accepted Manuscript*, which has been through the Royal Society of Chemistry peer review process and has been accepted for publication.

Accepted Manuscripts are published online shortly after acceptance, before technical editing, formatting and proof reading. Using this free service, authors can make their results available to the community, in citable form, before we publish the edited article. We will replace this *Accepted Manuscript* with the edited and formatted *Advance Article* as soon as it is available.

You can find more information about *Accepted Manuscripts* in the [Information for Authors](#).

Please note that technical editing may introduce minor changes to the text and/or graphics, which may alter content. The journal's standard [Terms & Conditions](#) and the [Ethical guidelines](#) still apply. In no event shall the Royal Society of Chemistry be held responsible for any errors or omissions in this *Accepted Manuscript* or any consequences arising from the use of any information it contains.

Cite this: DOI: 10.1039/c0xx00000x

www.rsc.org/xxxxxx

ARTICLE TYPE

Self-assembly polymorphism of 2,7-bis-nonyloxy-9-fluorenone: solvent induced the diversity of intermolecular dipole–dipole interaction

Lihua Cui, Xinrui Miao,* Li Xu, Yi Hu and Wenli Deng*

Received (in XXX, XXX) Xth XXXXXXXXX 20XX, Accepted Xth XXXXXXXXX 20XX

DOI: 10.1039/b000000x

In this present work, a scanning tunneling microscope (STM) operated under ambient conditions was utilized to probe the self-assembly behavior of 2,7-bis-nonyloxy-9-fluorenone (F-OC₉) at the liquid–solid (l/s) interface. On the high-oriented pyrolytic graphite (HOPG) surface, two-dimensional (2D) polymorphism with diversity of intermolecular dipole interaction induced by solvent was found. Solvents ranged from hydrophilic solvating properties with high polarity, such as viscous alkylated acids, to nonpolar alkylated aromatics and alkanes. 1-Octanol and dichloromethane were used to detect the assembly of F-OC₉ at the gas–solid (g/s) interface. The opti-electronic properties of F-OC₉ were determined by UV-Vis and fluorescence spectroscopy in solution. Our results showed that there were tremendous solvent-dependent self-assemblies in the 2D ordering for the surface-confined target molecules. When homologous series of alkanic acids ranged from heptanoic to nonanoic acid were employed as solvents, the self-assembled monolayer evolved from low-density coadsorbed linear lamellae to a semi-circle like pattern at the relative high concentrations, which was proved to be the thermodynamic state as it was the sole phase observed at the g/s interface after the evaporation of solvent. Moreover, by increasing the chain length of the alkylated acids, the weight of the carboxylic group, also being the responsible group for the dielectric properties, diminished from heptanoic to nonanoic acid, which could make the easier/earlier appearance of linear coadsorption effect. However, this was not the case for nonpolar 1-phenylotane and *n*-tetradecane: no concentration effect was detected. It showed strong tendency to aggregate into the coexistence of separate domains of the different phases due to the fast nucleation sites. Furthermore, thermodynamic calculations indicated that the stable structural coexistence of the fluorenone derivative was attributed to the synergetic intermolecular dipole–dipole and van der Waals (vdWs) forces at l/s interface. It is believed that the results are of significance to the solvent induced polymorphism assembly and surface science.

1. Introduction

The performance of the organic electronic devices is dependent on the opto-electric properties of fluorine- or fluorenone- based materials.^{1–7} It is now established that, besides the “primary” chemical nature of the molecules, the polymorphism arranged in the solid state has a strong influence on the opto-electronic property.^{8–9} For instance, the predominant properties of organic field effect transistors arise from the organization of the conjugated molecules in the very first monolayers deposited on top of the dielectric surface, as a result of the occurrence of the charge transport through a thin conducting channel at the semiconductor–insulator interface.¹⁰ In the past few years, it has been shown that investigation of the thin layers of the conjugated polymers or oligomers can help to understand and further control the supramolecular assembly in the application of constructing functional nano-devices.^{11–16} With respect to the nano-devices, not only the properties of individual molecules but also the conformation, orientation and packing structures of these molecules could be effective in the performance of the molecular devices.^{17–18} Therefore, it is desirable to understand and control the 2D self-assembled structural polymorphism and the properties of surface-confined molecules.¹⁹

It is well demonstrated that the supramolecular assemblies on

highly oriented pyrolytic graphite (HOPG) surfaces are sensitive to the delicate balance, *e.g.*, the intermolecular interaction between the adsorbed molecules and molecule–substrate interaction,²⁰ which is usually in the form of weak and reversible non-covalent forces such as the hydrogen-bonding, vdWs, dipolar, electrostatic, metal–ligand coordination and π – π stacking.^{21–26} In addition, various parameters including polarity of solvent,^{27–28} concentration,^{29–31} temperature,^{32–34} dielectric³⁵ and molecular ratios³⁶ have been proven to be effective in the phase transformations of the 2D self-assembled supramolecular architectures. Among all the important parameters for self-assembly at the l/s interface, the solvent is believed to take effect in the assembled processes through the coadsorption or solvation in some alkyl substituents of the molecules.^{30, 37–38} The nature of solvent with the aspect of physical and chemical properties has been extensively used to tune the molecular self-assembled structures.^{39–40} Chemical properties (aromatic interaction, odd-even effect, saturated and unsaturated solvent, and the length of alkyl chain) and physical properties of solvent (solubility, hydrophilic and hydrophobic properties, polarity, dielectric constant and viscosity) are crucial for the extensively explored solvent-induced polymorphism.⁴¹ In most cases, solvent molecules with approximate size can be coadsorbed in the molecular network.^{34, 42–43} Sometimes the concentration and the sort of solvents could affect the molecular coverage and the self-

assembly pattern in one building block,^{29, 44-45} thus it is a great challenge to predict the thermodynamic equilibrium structure for a particular system.

In our previous paper, the odd-even alkoxy chain length effect in 2,7-bis(*n*-alkoxy)-9-fluorenone (F-OC_{*n*}, *n* = 12 to 18) was investigated.⁴⁶ Solvent-responsive 2D morphology of F-OC₁₃ were obtained resulting from adsorbate-solvent interaction.⁴⁷ The molecular size, shape and structure of molecular substituents were key factors in regulating the balance of the intermolecular dipole-dipole and vdWs interaction and formation of self-assembled structures.²² However, as the long side chains *n* = 12 to 18 yield the large vdWs interaction of intermolecular (mainly from alkyl-alkyl) and the alkyl chains-substrate, we shortened the side chains to detect the delicate competition between dipolar and vdWs interactions. Also a series of comparison in the solvent effect between the homologous alkyl acids were given.

Table 1. Physical properties of the solvents used

chemicals	Boiling point (°C)	Viscosity (mN s m ⁻²)	Dielectric constant (ε/ε ₀)	Dipole moment (Debye)
1-phenylotane	261–263	2.61	2.26 (20)	0 / 0.6602
<i>n</i> -tetradecane	254	2.18	2.01 (20)	0.0002
dichloromethane	240	0.43	6.49 (20)	3.40
1-octanol	195	6.13	10.3 (20)	1.72
heptanoic acid	222–224	2.72	3.04 (30)	1.57
octanoic acid	237	4.20	2.82 (30)	1.50
nonanoic acid	253	7.25	2.59 (22)	1.32

In this paper, for the assembly of F-OC₉, we choose types of solvents ranging from those hydrophilic solvating properties with high polarity, such as viscous alkylated acids, to nonpolar solvents such as alkylated aromatics and alkanes. In addition, volatile 1-octanol and dichloromethane are introduced to detect the thermodynamic stable state after the evaporation of solvent. Chemical structures of the solvents (Table S1) and their physical properties used in this work are listed in Table 1. High-resolution STM images fully reveal the solvent-responsive 2D morphologies of F-OC₉ dissolved in seven representative solvents: 1-phenylotane, *n*-tetradecane, 1-octanol, dichloromethane, heptanoic acid, octanoic acid and nonanoic acid. When the solution is diluted to a low concentration (~10⁻⁶ mol L⁻¹), of particular interest was the fact that in polar solvents (alkylated acids), solvent molecules can be coadsorbed in the molecular network attributed to the hydrogen bonding and striking influence of the alkyl chain length. Moreover, as the chain length of alkylated acids increases, the weight of the carboxylic acid group (also being the responsible functional group for the dielectric properties) diminishes from heptanoic to nonanoic acid. Therefore, the 2D supramolecular patterns are affected accordingly. On the other hand, the nonpolar solvent is expected to enhance the number of nucleation sites, thus leading to small

domains. No concentration effect was observed in the nonpolar environment. The different energy among different polymorphs determines the system sensitivity towards concentration. The larger the energy difference, the more dramatic the concentration dependence. When the volatile 1-octanol and dichloromethane are used as the solvents, the thermodynamic stable semi-circle like pattern is favored, which is the same as that obtained at the l/s interface. Herein, the solvent-dependent supramolecular assembled behavior is confirmed and discussed in terms of the nature of solvent, solvent-solute and intermolecular interactions. UV-Vis and fluorescence spectra serve as a further confirmation owing to the wavelength shifts of the characteristic peaks. Furthermore, to interpret and confirm the synergetic effect of the molecule-molecule interactions dominated by the dipole-dipole and vdWs forces, corresponding simulations and calculations are carried out, which fit the experimental results quite well.

2. Experimental Section

2,7-Bis-nonyloxy-9-fluorenone (F-OC₉) used in this study was synthesized as described in previous report.⁴⁷ It was obtained by the repeated recrystallization in order to ensure the purity. 1-Phenylotane, *n*-tetradecane, 1-octanol, dichloromethane, heptanoic acid, octanoic acid and nonanoic acid were used as received from Aldrich without further purification. The samples were prepared by adding a droplet of the solution contained F-OC₉ at a concentration between 10⁻⁴ and 10⁻⁵ M onto a freshly cleaved atomically flat surface of HOPG (quality ZYB, Bruker, USA). The images obtained at the l/s interface were recorded within 2 h after dropping a solution of the F-OC₉. In order to investigate the assembly of F-OC₉ at g/s interface, the samples were rescanned after replaced 2–4 h or even longer. STM measurements were performed at the ambient conditions with the tip immersed in the supernatant liquid using a Nanoscope IIIa Multimode SPM (Bruker, USA). The tips were prepared by the mechanical cutting from Pt/Ir wire (80/20, diameter ~ 0.2 mm). All the STM images were obtained by the current mode of operation. Each specific tunneling condition was given in the corresponding figure captions. All the experiments were repeated in several sessions with different tips and samples to check the reproducibility and to exclude experimental artifacts caused by them. It is convenient to determine the average lattice parameters of the F-OC₉ monolayer using the HOPG lattice as an internal standard to correct each scanning image by examining at least 4 images. Our images were shown without further processing except flattening to move the tilting effect of the HOPG substrate plane. UV-Vis spectra were investigated with an UV-3010 UV-Visible spectrophotometer (Hitachi, Japan) from 800 to 200 nm. Fluorescence spectrum was recorded by an F-4500 fluorescence spectrophotometer (Hitachi, Japan).

Molecular models of the assembled structures were performed with Materials Studio (MS) 5.5. The models of the monolayers were reliable, because they were constructed according to the intermolecular distances and angles by the analysis of the STM images. Calculations of the spatial distribution of the HOMO (Fig. S1), dipole moment and energy of F-OC₉ were conducted with the density functional theory (DFT) as implemented in the DMol3 package. Perdew-Burk-Ernzerh (PBE) function was used to describe the exchange and correction. All of the computations

were all-electron spin restricted ones and were performed with minimal basis set and medium integration mesh. The convergence thresholds for energy and electron density in self-consistent iterations are 1.0×10^{-5} a.u. and 1.0×10^{-3} a.u. for gradient and displacement in geometry optimizations.

3. Results

3.1 Solvent-induced polymorphism and coadsorption of F-OC₉ at alkylated acids/HOPG interfaces

3.1.1 Concentration dependent structural transition in heptanoic acid

The monolayer formation of F-OC₉ is investigated at the heptanoic acid/HOPG interface under different solution concentrations (from 10^{-4} to 10^{-6} mol L⁻¹) to evaluate the effect of the solution concentration on the 2D geometries. Fig. 1 shows the assembly of F-OC₉ and the corresponding tentative molecular models at high concentrations (10^{-4} – 10^{-5} mol L⁻¹). In the STM images, the fluorenone moieties are observed to be bright gemmiform features owing to the high tunneling efficiency. The stripe features between the fluorenone moieties correspond to alkyl chains. The orientation of fluorenone groups can be identified by the HOMO level. The high-resolution STM image (Fig. 1b) shows the structural details of the semi-circle like pattern. Five F-OC₉ molecules form a pentamer as the basic unit of the adlayer, as indicated in a solid green oval in Fig. 1b. Seen from the basic unit, there are two pairs of dimeric fluorenone groups, which arrange with a back-to-back configuration as shown in blue/pink hollow ovals, and the remaining F-OC₉ molecule occupies the space between adjacent tetramers. Careful observation shows that for the pentamers in adjacent lamellae, the side chains of F-OC₉ (indicated by the pink oval) arrange tail-to-tail and the side chains in other two molecules (indicated by the oval) are interdigitated. Regular distributions of voids can be observed. On the basis of the STM observation, a structural model for the semi-circle like pattern is proposed in Fig. 1d. The parameters of the unit cell outlined in Fig. 1b are $a = 2.4 \pm 0.2$ nm, $b = 2.3 \pm 0.1$ nm, and $\alpha = 93 \pm 1^\circ$.

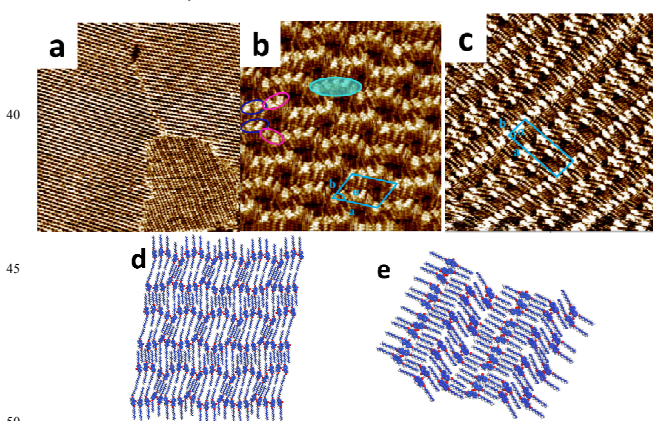


Fig. 1 Assembled structures of the F-OC₉ molecule in heptanoic acid (2.5×10^{-4} mol L⁻¹) on the HOPG surface. (a) Large-scale STM image of the coexistence of different structures. (Scan area: 200×200 nm². $V_{\text{bias}} = 769$ mV, $I_t = 473$ pA). High-resolution images showing (b) the semi-circle like pattern and (c) alternating pattern. (Scan area: 20×20 nm²). (d, e) Molecular models illustrating the self-assembly patterns based on the STM images for b and c respectively.

The well-ordered alternating pattern can be revealed in the high-resolution image (Fig. 1c). Trimeric and tetrameric bright lines appear alternately. The trimeric line is identical to the homologous assembled pattern of F-OC_{odd} in octanoic acid.⁴⁶ In the tetrameric line, each lamella consists of two molecular rows. In one row two molecules form a dimer with a back-to-back configuration and arrange with adjacent dimers in another row by a head-to-head fashion. It is worth mentioning that the arrangement of trimeric line is simply the result of shape complementarity with the tetramers-row lamella reinforced by the vdWs interactions between the side chains. The unit cell is superimposed on the high-resolution image in Fig. 1c with $a = 5.4 \pm 0.1$ nm, $b = 2.7 \pm 0.2$ nm, and $\alpha = 78 \pm 1^\circ$. The molecular density is 1.12 nm⁻², which is lower than the semi-circle like structure (1.81 nm⁻²).

When the solution concentration decreases to 10^{-5} – 10^{-6} mol L⁻¹, the whole scanning area is averaged by a uniform butterfly pattern as shown in Fig. 2a. The high-resolution STM image provides the detailed information for the assembled structure (Fig. 2b). Every four F-OC₉ molecules form a tetramer that consists of two dimers. Two alkoxy chains in one F-OC₉ molecule are parallel to each other. The fluorenone groups in each tetramer arrange by a shoulder-to-shoulder fashion. Two dimers in one tetramer adopt a back-to-back fashion and form a butterfly pattern. Note that shorter chains could be seen in the image. On the basis of the length and the shape, these short chains are attributed to 1-heptanoic acid molecules coadsorbed with the F-OC₉ molecules. The unit cell of the 2D assembly is superimposed on the image in Fig. 2b with parameters $a = 2.8 \pm 0.2$ nm, $b = 2.6 \pm 0.1$ nm, and $\alpha = 111 \pm 1^\circ$. From the molecular arrangement and intermolecular distance, a structural model can be proposed in Fig. 2c. The formation of tetramers might involve hydrogen bonding between the carbonyl group of the F-OC₉ molecule and the carboxyl acid of heptanoic acid molecule, which is effective in generating the featured hydrogen bonded tetramer assembly.

One particularly interesting result for the above discussed assembly is that, after being scanned for several times by the STM tip, the butterfly pattern can be transformed into an alternating phase (Fig. S2). Simultaneously, the majority of the surface becomes covered by a homologous domain of this alternating pattern. Following consecutive scanning, the whole scanned area is covered by the alternating pattern. Here the alternating patterns with high density are formed from relatively concentrated solution of F-OC₉ and the most stable structures over a wide concentration range (10^{-5} to 10^{-6} mol L⁻¹), while it is the sole morphology coexisting with the butterfly structure observed at medium concentration. Systematic concentration dependent experiments reveal that there is considerable overlap in the concentration. Over which, the butterfly and alternating patterns are stable, and they can coexist.

At low solution concentrations, F-OC₉ could assemble into a coadsorbed linear structure at the heptanoic acid/graphite interface (Fig. 2d and e). The structural details revealed by a high-resolution STM image (Fig. 2e) show that the fluorenone moieties pack in a linear sequence in each lamella, and the alkyl chains in adjacent lamellae arrange in a tail-to-tail fashion. The angle between the directions along fluorenone moieties sequence and the lamellar axis is $89 \pm 2^\circ$. A careful observation reveals that

the sequential head-to-tail arrangement of fluorenone cores separates neighboring molecular dipole pairs to enhance dipole-dipole interaction thus lowering the electronic potential in a lamella (Fig. S3 and S.10). Similarly, the fluorenone cores in adjacent lamellae are arranged sequentially in the opposite direction. By counting the number of the chains and the side chains of F-OC₉, we find that the heptanoic acid molecules coadsorb on the HOPG surface, which can be revealed in the molecular model (Fig. 2f). The interdigitated solvent molecules can occupy the space resulting from the hydrogen bonding and steric matching. Due to the asymmetry induced by the hydrogen bonding, the fluorenone cores in each lamella do not pack in a strict line. The unit parameters are $a = 1.6 \pm 0.1$ nm, $b = 3.1 \pm 0.2$ nm, and $\alpha = 80 \pm 2^\circ$. A structural model for the adlayer is sketched in Fig. 2f, which is consistent with the STM results.

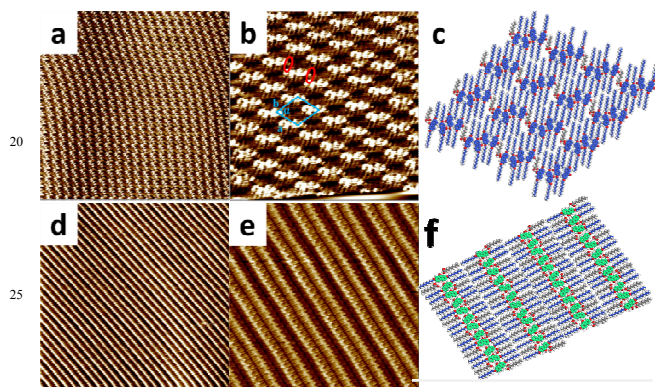


Fig. 2 (a) Large-scale (100×100 nm²) and (b) high-resolution (20×20 nm²) STM images of the F-OC₉ self-assembled monolayer in heptanoic acid at a medium concentration of 3.5×10^{-5} mol L⁻¹. ($V_{\text{bias}} = 630$ mV, $I_t = 505$ pA). (d) Large-scale (200×200 nm²) and (e) high-resolution (37×37 nm²) STM images of the F-OC₉ self assembled monolayer in heptanoic acid with a low concentration (7.5×10^{-6} mol L⁻¹). ($V_{\text{bias}} = 630$ mV, $I_t = 520$ pA). (c, f) Molecular models of butterfly and linear structures based on (b) and (e) respectively.

The results show that the assemblies of F-OC₉ can vary with the change of solution concentration in the same solvent. At low concentrations, the solvent could be coadsorbed with F-OC₉ molecule. The assembled structures of F-OC₉ with different conformations in a unit cell have different contact areas with the surface, which can result in a difference in adsorption energy, and in turn lead to preferential adsorption. In view of the total energy, densely packed assembly is most frequently favored in which the adsorbate-adsorbate and adsorbate-substrate interactions could be maximized, especially when the intermolecular interaction lacks directionality. The average area per molecule (1.02 nm²) in the linear structure is larger than that (0.55 nm²) in the semi-circle pattern, which elucidates that the lower the concentration, the larger the chance to form a low density pattern.

3.1.2 Self-assembly in octanoic acid

At the octanoic acid/HOPG interface, F-OC₉ assembles into “lips” and semi-circle like structures at a medium concentration (Fig. S4a). From the high-resolution image of “lips” shaped pattern (Fig. 3a), the π -conjugated units and alkyl chains are alternately aligned in a zigzag mode. The length of dimeric bright

rod is 0.9 ± 0.1 nm, which corresponds to the length of a fluorenone group. According to the proposed model in Fig. 3b, two fluorenone cores form a dimer in a back-to-back fashion. It is supposed that such a dimer pattern is formed resulting from the length matching of the side chains and the conjugated moieties. The unit cell parameters of the network are determined to be $a = 1.7 \pm 0.1$ nm, $b = 1.6 \pm 0.1$ nm, $\alpha = 126 \pm 1^\circ$. It is inferred that the “lips” shaped pattern is as stable as the semi-circle like structure. A coadsorbed linear pattern was also observed for the self-assembly at the octanoic acid/HOPG interface under low concentrations of 10^{-6} mol L⁻¹ (Fig. S4b), which is identical to that assembled at heptanoic acid/HOPG interface.

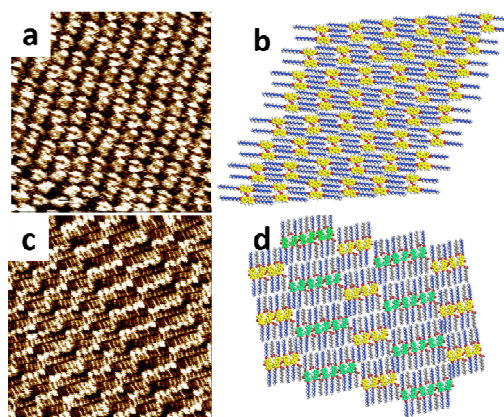


Fig. 3 (a) High-resolution STM image of F-OC₉ in octanoic acid at a medium concentration (5.8×10^{-5} mol L⁻¹). (Scan area: 200×200 nm². $V_{\text{bias}} = 630$ mV, $I_t = 505$ pA). (b) Molecular model for the “lips” shaped structure. (c) High-resolution STM image of F-OC₉ in nonanoic acid at a medium concentration of 1.3×10^{-5} mol L⁻¹. (Scan area: 200×200 nm². $V_{\text{bias}} = 650$ mV, $I_t = 500$ pA). (d) Molecular model for the dislocated tetramers and hexamers structure in (c).

3.1.3 Concentration-dependent coadsorption in nonanoic acid

Fig. 3c and S4 illustrate STM images recorded for the adlayer of F-OC₉ physisorbed at the 1-nonanoic acid/HOPG interface. At high concentrations, the most stable semi-circle like pattern is observed as that obtained in heptanoic and octanoic acids (Fig. S5a). With the decrease of the solution concentration, the high-resolution STM image (Fig. 3c) provides the detailed information for the self-assembly structure. From the molecular arrangement and intermolecular distance, it can be determined that every four or six F-OC₉ molecules form an aggregation that consists of two or three dimers respectively. Owing to the length matching effect between the side chains and the conjugated moieties, dimeric fluorenone groups are packed in a back-to-back fashion. Thus, the fluorenone moieties in adjacent coadsorbed tetramers and hexamers pack dislocatedly at the length of a nonane chain. A structural model for the adlayer is sketched in Fig. 3d. The unit cell can be defined with $a = 2.9 \pm 0.2$ nm, $b = 1.5 \pm 0.1$ nm, and $\alpha = 100 \pm 2^\circ$. Finally, similar to the low concentration in heptanoic and octanoic acids, the whole scanning area is covered by a uniform linear structure coadsorbed with the nonanoic acid (Fig. S5b).

3.2 Self-assembly in 1-phenyloctane and *n*-tetradecane

Experiments have also been performed in nonpolar solvents to

investigate the 2D molecular ordering of F-OC₉. In 1-phenyloctane or *n*-tetradecane, the nonpolar environment is expected to enhance the number of nucleation sites, thus leading to the coexistence of small domains. For more diluted solutions, no solvent molecules are coadsorbed, and in solution the states of existence of other assembled structures such as semi-circle nor “lips” shaped patterns don’t show detectable concentration dependence.

When using 1-phenyloctane as a nonpolar solvent with aromatic and aliphatic moieties, the adlayer is composed of three main domains denoted with I, II, and III (Fig. S6a and b), which are termed in the following high-resolution images denoted with as Fig. S6c–e, respectively. It is found that in 1-phenyloctane, the domain sizes for the phase I, II, and III are relatively small attributing to the fast nucleation rates. The coexistence of both polymorphs can be taken as an indication that the Gibbs energy is similar, and the average area per molecule (Table S2) demonstrates that the two patterns have the same stability on HOPG surface. Moreover, the three phases are all stable without apparent structural transformation of the F-OC₉ adlayer when concentration varies.

On the other hand, when adsorbed from nonpolar aliphatic *n*-tetradecane which is a good solvent for the aliphatic side chains but a poor solvent for the aromatic backbone, we can detect the coexistence of semi-circle and “lips” shaped phases shown in Fig. S7 just as the one found in 1-phenyloctane. Interestingly, a dislocated zigzag fashion is found to coexist with the semi-circle like pattern at the *n*-tetradecane/HOPG interface at medium concentrations ($\sim 10^{-5}$ mol L⁻¹) as shown in Fig. 4a. The high-resolution STM image (Fig. 4b) reveals the molecular packing details: two molecules form a dimer in a back-to-back fashion, and the adjacent dimers in a lamella pack with a dislocated arrangement. The unit cell can be defined with $a = 2.0 \pm 0.2$ nm, $b = 2.1 \pm 0.1$ nm, and $\alpha = 119 \pm 1^\circ$. The molecular model is proposed in Fig. c.

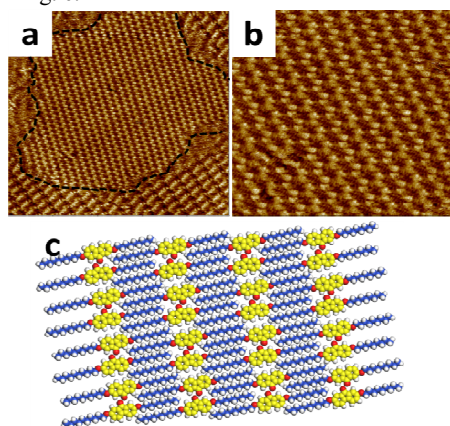


Fig. 4 (a) Large-scale (50×50 nm²) and high-resolution (20×20 nm²) STM images of F-OC₉ in *n*-tetradecane at a medium concentration of 1.3×10^{-5} mol L⁻¹. (Scan area: 200×200 nm². $V_{\text{bias}} = 701$ mV, $I_t = 598$ pA). (c) Molecular model of the dislocated zigzag model based on the image.

3.3 Self-Assembly of F-OC₉ after the evaporation of solvent

In order to decrease the effect of the solvent–molecule interaction on the self-assembled patterns of F-OC₉ on the HOPG surfaces, 1-octanol and dichloromethane are chosen as the volatile solvent.

The solvent could significantly affect the resulting self-assembled structure, thus we create a dry monolayer to identify the molecule–solvent and molecule–substrate interactions. The STM experiments are carried out within 3 h. Only the semi-circle like phase is observed (Fig. S7). It displays the large-scale most stable states. Except this, we could not detect “lips” or semi-circle like patterns indicating the semi-circle pattern is more stable. Due to the principle of closest packing, the denser semi-circle structure is likely the most thermodynamically stable among these monolayer polymorphs.

3.4 The optic-electronic properties of F-OC₉

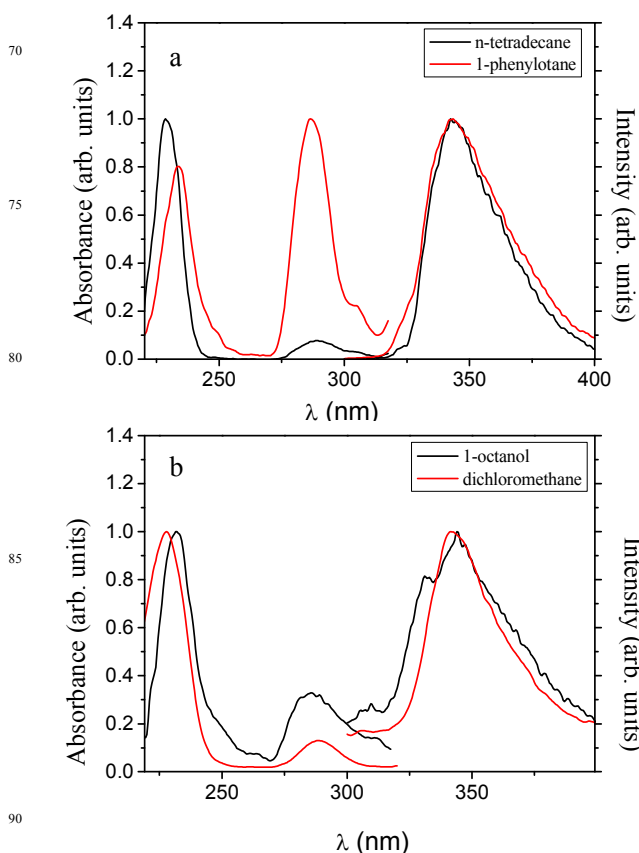


Fig. 5 UV-Vis absorption (left) and fluorescence spectra (right, excited with 228 nm) of F-OC₉ in (a) 1-phenyloctane and *n*-tetradecane; (b) dichloromethane and 1-octanol, respectively.

UV-Vis and fluorescence spectroscopy are effective optical characterization tools for understanding the electronic structure of fluorenone derivatives.^{48–51} They are also used to discern the electronic structure nature of F-OC₉ dissolved in the employing solvents in this study. Fig. 5 (a) and (b) show the typical examples of the solvent effects on the electronic absorption and emission spectra of F-OC₉ in 1-phenyloctane, *n*-tetradecane, dichloromethane and 1-octanol. The electronic absorption spectra contain two groups of bands stretching from 220 to 320 nm⁵² (two maxima at region 1 λ_{max} 228–234 nm and region 2 λ_{max} 285–288 nm). The characteristic peaks observed in Fig. 5a and b are assigned to π – π^* electron transitions. It is inferred that the observed spectral shift is correlated with the polarity parameters (dielectric constant and refractive index) of solvents.⁵¹ It is observed that F-OC₉ in 1-octanol exhibit a red-shift fluorescence

compared with that in dichloromethane. On account of the polarity of 1-octanol and dichloromethane (1-octanol > dichloromethane, Table 1), the red-shift of π - π^* electron transition in F-OC₉ spectrum with 1-octanol as the solvent implies that F-OC₉ in increasing polar solvent can absorb the ultraviolet light with the longer wavelength. The relative changes can also be confirmed by the fluorescence emission spectra shown in the right of Fig. 5 and Fig. S10. Obviously, F-OC₉ only displays a strong emission peak at about 342 nm. The shifts of π - π^* electron transitions are attributed to the different circumstances of the solvents used. The inducement in the dipole moment and nature of the solvent can cause changes to the excited state of substituted fluorenones, and therefore causes the differences in these UV-Vis and fluorescence spectra.

4. Discussion

4.1 Effect of coadsorption

At the *l/s* interface, there is an equilibrium between the molecules (or coadsorbed solvent) adsorbed on the surface and those which go back into the solution. In general, the molecule-substrate interaction drives the conjugated core or alkyl chains of molecules to adsorb on the substrate. Especially when the solvent contains donors or acceptors, the solvent can be coadsorbed at the *l/s* interface via the space matching, vdWs interaction or hydrogen bonding with the adsorbates. Intermolecular interaction makes the molecules form a close-packed adlayer to decrease the total energy in the system. For the assembly of F-OC₉ dispersing in alkylated acids, the same coadsorbed lamellar structure at low concentrations is observed independent of the analogues of linear alkyl acids. Therefore, solvent molecules coadsorbed on the side chain lamella are part of complex 2D assembled structures. With the variation of alkyl acids at the medium concentrations, due to the polarity of the fluorenone cores, F-OC₉ tends to arrange in different orientations aiming to achieve the lowest energy. The difference between the butterfly (Fig. 2b), linear (Fig. 2e), dislocated tetramers and hexamers (Fig. 3d) patterns in the coadsorption behavior of alkylated acids is a result of hydrogen-bonding and packing constraints. However, in aromatic alkylated solvents and *n*-alkanes, no solvent coadsorption can be observed. The coadsorption morphology involves hydrogen bonding between the carbonyl group of F-OC₉ molecule and the carboxyl acid of the solvent molecules, which is significant in engendering the featured hydrogen bonded assembly. Besides, it is the result of shape complementarity with the collinear lamellae or steric constraints reinforced by the underlying substrate interactions. The presence of the solvent coadsorption further stabilizes the highly alternating assemblies, i.e., a particular solvent stabilizing a particular modification by lowering its free energy.

Furthermore, in view of the geometric characteristics, the adsorption structures and unit cell parameters of different assembled patterns of the physisorbed adlayers of F-OC₉ at homologous acids/HOPG interfaces described in Table S2, an obvious feature of the self-assembly of F-OC₉ monolayer at the *l/s* interface is the earlier/easier appearance of F-OC₉ dissolved in nonanoic acid. Correspondingly, the possible straightforward rationalization to explain the observed solvent coadsorption effect is that a particular solvent stabilizes a particular modification by changing the assembly polymorphism to lower its Gibbs free

energy. We define the reason can be the reliance on the association constants of the monocarboxylic acids, which is known to be inversely linear to the dielectric constants.

4.2 The nature of solvents: polarity of environments and the varying solubility, viscosity, polarity and dielectric constants in homogeneous alkylated acids

From the comparison of schematic adsorption geometric representation of F-OC₉ dissolved in nonpolar and polar solvents in Table S2 in combination with the physical properties of solvent as stated in Table 1, F-OC₉ is always well dispersed in the alkylated acids, and the same coadsorption structure at low concentrations is observed independent of the analogues of linear alkyl acids. It is commonly known that the microenvironment of the adsorbates can be tuned by the polarity of the solvents, thus it seems reasonable to assume a disparate mechanism for the formation of the interfacial monolayers depending on the polarity of the solvents. Generally, solvents have an important impact on the molecular geometries, electronic structures and reaction mechanism (S.10). Based on the reaction field theory from Onsager (Fig. S9), the solute is placed in a spherical cavity. The hole is surrounded by a continuous medium with a certain dielectric constant ϵ_s . One of the noticeable points is that the directionality of dipole moment in the alkyl acids with carboxylic group plays a key role in the 2D organization. F-OC₉ molecules are polarized, with dipole moment induced. It could be envisaged that the ordered arrangement of the solvent molecules can introduce localized asymmetrical chemical environments as a result of the interference of solute molecules. This induction force in turn produces a net effect of increasing stability because of the interaction between the solute molecules and polar solvent. For alkanes and arylalkanes like 1-phenyloctane and *n*-tetradecane, solvent deviations from the predictions based on the dielectric constant are attributed to the lack of any polar anchor group to induce orientation by hydrogen bonding. Here it appears that no concentration dependent effect occurs at the interface, and nonpolar solvent is expected to enhance the number of nucleation sites, thus leading to the coexistence of different small domains. The polar solvents could induce the self-assembly polymorphism according to the solvent-molecule interaction in form of the hydrogen bonding and steric constraints. Seen from the assembly of F-OC₉ dissolved in homogeneous alkylated acids (Table S2), F-OC₉ monolayer density decreases in the first appearance of butterfly phase (0.92 nm⁻²) assembled at the heptanoic acid/HOPG interface and coadsorbed linear phase (0.88 nm⁻²) assembled at the octanoic acid/HOPG interface, compared with the density in the dislocated tetramers and hexamers phase (0.84 nm⁻²) assembled at the nonanoic acid/HOPG interface. In combination with the solvent properties described in Table 1, it is reasonable to assume a disparate mechanism for the formation of the interfacial monolayer structures depending on the varying solvent nature. The reason for the easier and earlier appearance of solvent coadsorption of the alkyl acids molecule in nonanoic acid can be related to the kinetic effects (From the basic consideration, adsorption rate of the solute molecules is proportional to c/η , where c stands for the concentration of solute and η for the viscosity), e.g., solubility thus the desorption rates. Besides, the dielectric properties of the solvent used are of significance. Firstly, the general trend of alkanolic acid (from heptanoic to

nonanoic acid) in solution can be effective in the assembly of F-OC₉. It is known that the longer chain length of a fatty acid results in the more hydrophobic liquid.³⁵ As the length of the aliphatic tail of solvent molecules increases from heptanoic to nonanoic acid, the solubility decreases (the molecule–molecule interaction and thus the viscosity of the respective functional group rises). As a result, this leads to the decrease of the diffusion constant of F-OC₉. A more densely packed arrangement would be favored for a higher adsorption rate, for the fast association of the molecules does not allow the system to adopt the structure with the lowest free energy. For example, it was reported that in UHV deposition experiment of TMA, the assembly structure was related to the adsorption rate, i.e., higher deposition rates led to a preference of the denser flower structure.⁵³

Secondly, the general trend of observing a higher symmetrical arrangement of the fluorenone derivatives on the basis of these solvents can readily be explained by invoking the principle of polarity. As discussed above, easier solvent coadsorption of the alkyl acids could induce the self-assembly polymorphism attributed to the different solvent–molecule interactions, especially in nonanoic acid. The dielectric constant of the solvents used is known to take effect in dictating the properties of alkanolic acids.³⁵ Even more important is the fact that the lower analogues of linear alkyl acids tend to exist as multimers, e.g., formic acid trimer⁵⁴ and pentamers⁵⁵ proved to be stable according to ab initio calculations. The enhanced hydrophobic effects will drive the polar carboxylic acid groups to assemble or aggregate in a less polar fashion due to the long chains, which will minimize electrostatic effect in solution. Thus the dimers with zero dipole moment tend to be formed in alkyl acids with longer chain lengths, which will lead to a stabilization of the carboxylic acid groups in a hydrophobic environment with low dielectric constant.^{56–57} This is because the molecular weight of the carboxylic acid group diminishes from heptanoic to nonanoic acid. As the association constants of aliphatic monocarboxylic acids are known to be inversely linear to the dielectric constants, the dielectric constant (ϵ) decreases along the homologous series from heptanoic acid (3.04) to nonanoic acid (2.59). For those assembly of F-OC₉ dissolved in acids, the easier occurrence of less polar and less dense arrangement is generated in the case of the more hydrophobic nonanoic acid, whereas the more polar and denser alternating phase is materialized with the more polar heptanoic acid. The dislocated tetramers and hexamers phase formed by dimers exposes loose packed and lower polar group, and this structure is clearly preferred in a solvent of low dielectric constant and vice versa.

Moreover, the nature of solvents differs in the homologous acids (Table 1), it is worth mentioning that over the scan time, the assembly of F-OC₉ will eventually, nevertheless, be dominated by the same semi-circle like pattern at homologous acids/HOPG interfaces as observed at the g/s interface after the evaporation of solvent. The same dipole–dipole interaction in the semi-circle like pattern indicates that the evaporation rate of solvent does not affect the thermodynamic stable molecular dipole–dipole interactions of F-OC₉ at the l/s interface.

4.3 Thermodynamics of F-OC₉: the evolution from monomolecular stability to clusters

4.3.1 Intermolecular dipole–dipole interaction

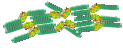
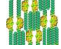
Table S2 summarizes the geometric characteristics, adsorption structures, unit cell parameters and packing density of the 2D assembled patterns of physisorbed adlayers observed in 2D assembly of F-OC₉. Structural models are schematically shown for all phases formed in this work. To describe each phase, representative aggregation modes for each phase are assigned to the building blocks constructed by two basic repeating units, as illustrated in Fig. 6b. Noncovalent interactions are satisfied to different extents in the two aggregates. Similar to 3,8-bis-hexadecyloxybenzo [c] cinnoline (BBC16),²⁷ F-OC₉ has a bent core that possesses a C_{2v} symmetry. First, F-OC₉ consists of a fluorenone core with strong polarity ($\mu = 3.5$ D) and alkoxy chains with weaker polarity originating from the different electron density induced by the electron-rich and electron-poor subunits. Second, the flexible alkoxy chains can change chains' direction to form the parallel close-packed adlayers. Third, adsorption-induced asymmetric assembly was reported in the case of BBC16 SAMs, due to the alkoxy chain distortion upon adsorption on the surface. The flexible conformational nature is effective in determining 2D crystal structure. If they are stable, each is expected to generate a different pattern during the assembly process.

Generally, the molecular dipole moment tends to arrange in collinear and antiparallel modes to maximize the dipole–dipole interaction⁵⁸, as schematically shown in Fig. 6. In order to interpret the intermolecular dipole–dipole interactions, we visualize each schematic structure in Fig. 6b. From the theoretical calculated dipole moments, it is demonstrated that the singular molecular conformation is calculated to be $\mu = 3.3$ D. For the dimers, the antiparallel arrangement of the molecular dipole of fluorenone units could avoid the potential dipole repulsions (S.11). The dipole moment of the dislocated antiparallel pattern decreases to be 0.26 D, which is also obviously less than that of singular molecule. As the case to trimers, the dipole moment decreases to 0.309 D. The calculation results reveal that the intermolecular dipole–dipole interaction contributes to the molecular arrangement. Moreover, our theoretical estimations confirm that the dipole arrangements of fluorenone moieties in the experimental self-assembly patterns are energetically favored. The alternating, “lips” and semi-circle shaped patterns are all stable which could justify the equal chance of obtaining these self-assembly patterns both in the experiments and theoretical calculations. Thus the variance of these assembled structures must be related to the synergetic effect of intermolecular interaction between dipole–dipole and vdWs forces.

4.3.2 Synergetic effect of molecule–molecule interactions dominated by dipole–dipole and vdWs forces

When the solvent is evaporated completely or the solution is at high concentrations, the molecule–solvent interaction is inexistence or very weak. A balance between intermolecular vdWs interaction of side chains and the dipole–dipole interaction of fluorenone groups mainly dominates the assembly of F-OC₉. By way of illustration we refer to the assembly of F-OC₉ dissolved in 1-phenylotane. The coexistence of alternating and “lips” shaped patterns is a result of thermodynamic balance of

Table 2. Comparison of unit cell parameters, molecular packing density of the alternating and “lips” shaped patterns of F-OC₉ self-assembled at the 1-phenylotane/HOPG interface

Type	Structural model	Unit cell parameters			Molecules per symmetric unit	S (nm ² per molecule)	Dipole moment (Debye)	Dipolar interaction (kJ mol ⁻¹)	vdWs interaction (kJ mol ⁻¹)
		a (nm)	b (nm)	α (°)					
I		5.4 ± 0.1	2.5 ± 0.2	80	7	0.82	0.7956	13.69	40.50
II		1.8 ± 0.2	1.6 ± 0.2	125	2	0.89	0.2562	18.53	35.14

intermolecular vdWs and dipole–dipole interaction. Numbers for the dipolar contribution to the enthalpic gain for alternating and “lips” shaped patterns respectively are provided in Table 2. It can be clearly seen that the alternating structure is less favorable than the “lips” shaped structure. However, the situation is altered when the calculated packing density is taken into account. In this case, the chain–chain vdWs interaction (S.12) may be predominant during the synergetic process.

It is inferred that the vdWs interaction energy is 40.5 kJ mol⁻¹ for the alternating pattern, which is larger than “lips” shaped pattern (35.143 kJ mol⁻¹). From the enthalpic point of view³⁴, this alternating arrangement is one, if not the, least stable arrangements possible than the “lips” shaped pattern. The result suggests that for the densely packed alternating and “lips” shaped structures, the vdWs force is the main contributor than the dipole–dipole interaction. Moreover, the calculated similar enthalpic gain for the two structures verifies the coexistence of different phases and there is no concentration effect in nonpolar solvents. The difference of energy between both polymorphs determines the system sensitivity towards concentration: the larger the energy difference, the more dramatic the concentration dependence. As these two assemblies (semi-circle and “lips” shaped patterns) are very close in energy, and there is no asymmetry induced effect in nonpolar solvent, they locally coexist on the surface. However, we cannot simulate the assembly patterns on HOPG by direct MD in this case employing the popular energy minimization methods to give more insight, owing to the importance of thermal and entropic factors in the affinity of F-OC₉ and coadsorbed solvent molecules.

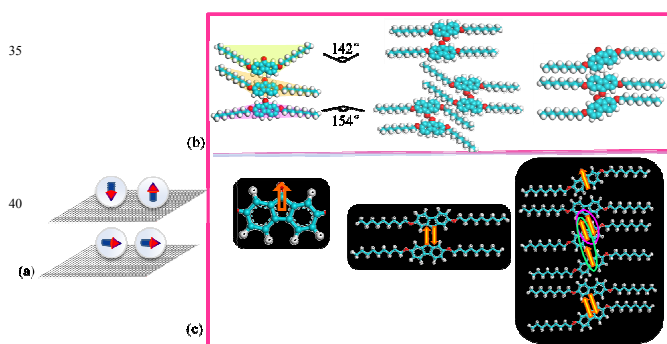


Fig. 6 (a) Typical configurations of one and two nanoparticles on the graphite surface are shown. Collinearly arranged and antiparallel arranged dipoles are most stable states. (see supporting information S. 11). (b) Molecular structure of F-OC₉ and aggregation modes experimentally observed. (c) Schematic diagram for the molecular assembly model for singular without side chains for F-OC₉ in the original structure, and the detailed dipolar interaction of molecular models for the dimers and trimers shown in (b).

5. Conclusion

In summary, 2D supramolecular self-assembly of F-OC₉ at the l/s interface was shown to depend on the polarity of solvents. When the polar acids were employed as solvents, the asymmetry environment induced the monotonous structure. With the decrease of F-OC₉ concentration, coadsorption was observed attributed to the hydrogen bonding and steric constraints. On the other hand, the fast nucleation rate led to the coexistence of small domains. No concentration effect was found due to the nonpolar environment. In addition, the difference in coadsorption behavior of homologous acids was understood on the basis of dielectric variance among the alkylated acids. At l/s interface, the thermodynamics of fluorenone derivative was rationalized in terms of the specific noncovalent stabilizing intermolecular interactions of synergetic dipole–dipole and vdWs forces. Thermodynamic state at the g/s interface was the same as that at l/s interface, which indicated that the semi-circle like pattern was dominated by the intermolecular interaction rather than the solvent. In addition, the absence of characteristic peaks and the shifts of π–π* electron transitions in UV-Vis and fluorescence spectra implied that changes in the dipole moment and nature of the solvent can cause significant changes to the excited state of substituted fluorenes. An understanding of the solvent effects on the current system will allow us to direct and control the molecular ordering of the 2D physisorbed monolayers, which is important for the tunable design of molecular materials and molecular electronics.

Acknowledgements

We thank J. Zhang for the help with experimental technique applied in UV-Vis and fluorescence measurements. Financial supports from the National Program on Key Basic Research Project (2012CB932900), the National Natural Science Foundation of China (21103053, 51373055, 21403072) and the Fundamental Research Funds for the Central Universities (SCUT) are gratefully acknowledged.

Notes and references

College of Materials Science and Engineering, South China University of Technology, Guangzhou 510640, China. E-mail: msxrmiao@scut.edu.cn, wildeng@scut.edu.cn; Tel: +86 (0) 20 22236708
 † Electronic Supplementary Information (ESI) available. See DOI: 10.1039/b000000x/

1 A. Goel, S. Chaurasia, M. Dixit, V. Kumar, S. Prakash, B. Jena, J. K. Verma, M. Jain, R. S. Anand and S. S. Manoharan,

- Org. Lett.*, 2009, **11**, 1289–1292.
- 2 J. H. Ahn, C. Wang, I. Perepichka, M. R. Bryce and M. C. Petty, *J. Mater. Chem.*, 2007, **17**, 2996–3001.
- 3 F. Lincker, N. Delbosc, S. Bailly, R. De Bettignies, M. Billon, A. Pron and R. Demadrille, *Adv. Funct. Mater.*, 2008, **18**, 3444–3453.
- 4 R. Demadrille, N. Delbosc, Y. Kervella, M. Firon, R. D. Bettignies, M. Billon, P. Rannou and A. Pron, *J. Mater. Chem.*, 2007, **17**, 4661–4669.
- 5 W. Porzio, S. Destri, U. Giovannella, M. Pasini, T. Motta, D. Natali, M. Sampietro and M. Campione, *Thin Solid Films*, 2005, **492**, 212–220.
- 6 W. Porzio, S. Destri, M. Pasini, U. Giovannella, R. Resel, O. Werzer, G. Scavia, L. Fumagalli, D. Natali and M. Sampietro, *Synth. Met.*, 2009, **159**, 513–517.
- 7 D. Yan, Y. Zhao, M. Wei, R. Liang, J. Lu, D. G. Evans and X. Duan, *RSC Adv.*, 2013, **3**, 4303–4310.
- 8 S. C. Simon, B. Schmaltz, A. Rouhanipour, H. J. Räder and K. Müllen, *Adv. Mater.*, 2009, **21**, 83–85.
- 9 H. Siringhaus, P. J. Brown, R. H. Friend, M. M. Nielsen, K. Bechgaard, B. M. W. Langeveld-Voss, A. J. H. Spiering, R. A. J. Janssen, E. W. Meijer, P. Herwig and D. M. de Leeuw, *Nature*, 1999, **401**, 685–688.
- 10 J. Puigmarti-Luis, A. Minoia, H. Uji-i, C. Rovira, J. Cornil, S. De Feyter, R. Lazzaroni and D. B. Amabilino, *J. Am. Chem. Soc.*, 2006, **128**, 12602–12603.
- 11 Y. Chang, H. Chen, Z. Zhou, Y. Zhang, C. Schuett, R. Herges and Z. Shen, *Angew. Chem. Int. Edit.*, 2012, **51**, 12801–12805.
- 12 H. Furuta, H. Nanami, T. Morimoto, T. Ogawa, V. Kral, J. L. Sessler and V. Lynch, *Chem. –Asia. J.*, 2008, **3**, 592–599.
- 13 S. Mohani and D. Bonifazi, *Coordin. Chem. Rev.*, 2010, **254**, 2342–2362.
- 14 J. S. Reddy and V. G. Anand, *J. Am. Chem. Soc.*, 2009, **131**, 15433–15439.
- 15 D. Wu, A. B. Descalzo, F. Weik, F. Emmerling, Z. Shen, X.-Z. You and K. Rurack, *Angew. Chem. Int. Edit.*, 2008, **47**, 193–197.
- 16 Z. L. Xue, J. Mack, H. Lu, L. Zhang, X. Z. You, D. Kuzuhara, M. Stillman, H. Yamada, S. Yamauchi, N. Kobayashi and Z. Shen, *Chem. –Eur. J.*, 2011, **17**, 4396–4407.
- 17 S. Weigelt, C. Busse, L. Petersen, E. Rauls, B. Hammer, K. V. Gothelf, F. Besenbacher and T. R. Linderoth, *Nat. Mater.*, 2006, **5**, 112–117.
- 18 X. M. Zhang, H. F. Wang, S. Wang, Y. T. Shen, Y. L. Yang, K. Deng, K. Q. Zhao, Q. D. Zeng and C. Wang, *J. Phys. Chem. C*, 2013, **117**, 307–312.
- 19 J. Puigmarti-Luis, A. Minoia, H. Uji-i, C. Rovira, J. Cornil, S. De Feyter, R. Lazzaroni and D. B. Amabilino, *J. Am. Chem. Soc.*, 2006, **128**, 12602–12603.
- 20 V. Palermo and P. Samori, *Angew. Chem. Int. Edit.*, 2007, **46**, 4428–4432.
- 21 L. Xu, X. R. Miao, B. Zha and W. L. Deng, *Chem. –Asia. J.*, 2013, **8**, 926–933.
- 22 L. Xu, X. R. Miao, X. Ying and W. L. Deng, *J. Phys. Chem. C*, 2012, **116**, 1061–1069.
- 23 T. Kudernac, S. Lei, J. A. A. W. Elemans and S. De Feyter, *Chem. Soc. Rev.*, 2009, **38**, 402–421.
- 24 S. Lei, K. Tahara, X. Feng, S. Furukawa, F. C. De Schryver, K. Muellen, Y. Tobe and S. De Feyter, *J. Am. Chem. Soc.*, 2008, **130**, 7119–7129.
- 25 L. Xu, L. Yang and S. Lei, *Nanoscale*, 2012, **4**, 4399–4415.
- 26 Y. Yang and C. Wang, *Chem. Soc. Rev.*, 2009, **38**, 2576–2589.
- 27 X. Shao, X. Luo, X. Hu and K. Wu, *J. Phys. Chem. B*, 2005, **110**, 1288–1293.
- 28 X. Zhang, H. Xu, Y. Shen, Y. Wang, Z. Shen, Q. Zeng and C. Wang, *Phys. Chem. Chem. Phys.*, 2013, **15**, 12510–12515.
- 29 C. Meier, M. Roos, D. Kunzel, A. Breittruck, H. E. Hoster, K. Landfester, A. Gross, R. J. Behm and U. Ziener, *J. Phys. Chem. C*, 2010, **114**, 1268–1277.
- 30 H. Nguyen Thi Ngoc, T. G. Gopakumar and M. Hietschold, *J. Phys. Chem. C*, 2011, **115**, 21743–21749.
- 31 K. S. Mali, M. G. Schwab, X. Feng, K. Mullen and S. De Feyter, *Phys. Chem. Chem. Phys.*, 2013, **15**, 12495–12503.
- 32 F. Hu, Y. Gong, X. Zhang, J. Xue, B. Liu, T. Lu, K. Deng, W. Duan, Q. Zeng and C. Wang, *Nanoscale*, 2014, **6**, 4243–4249.
- 33 C. Wang, P. K. Jana, H. Zhang, Z. Mu, G. Kehr, T. Blomker, G. Erker, H. Fuchs, A. Heuer and L. Chi, *Chem. Commun.*, 2014, **50**, 9192–9195.
- 34 M. O. Blunt, J. Adisoejoso, K. Tahara, K. Katayama, M. Van der Auweraer, Y. Tobe and S. De Feyter, *J. Am. Chem. Soc.*, 2013, **135**, 12068–12075.
- 35 L. Kampschulte, M. Lackinger, A. K. Maier, R. S. K. Kishore, S. Griessl, M. Schmittel and W. M. Heckl, *J. Phys. Chem. C*, 2006, **110**, 10829–10836.
- 36 Y. T. Shen, L. Guan, X. Y. Zhu, Q. D. Zeng and C. Wang, *J. Am. Chem. Soc.*, 2009, **131**, 6174–6180.
- 37 M. Lackinger and W. M. Heckl, *Langmuir*, 2009, **25**, 11307–11321.
- 38 J. Liu, X. Zhang, H. Y. Yan, D. Wang, J. Y. Wang, J. Pei and L. J. Wan, *Langmuir*, 2010, **26**, 8195–8200.
- 39 L. Y. Liao, X. M. Zhang, F. Y. Hu, S. Wang, S. D. Xu, Q. D. Zeng and C. Wang, *J. Phys. Chem. C*, 2014, **118**, 15963–15969.
- 40 D. Wang, L. J. Wan and C. L. Bai, *Mat Sci Eng R*, 2010, **70**, 169–187.
- 41 Y. L. Yang and C. Wang, *Curr Opin Colloid In*, 2009, **14**, 135–147.
- 42 L. H. Cui, X. R. Miao, L. Xu and W. L. Deng, *Appl. Surf. Sci.*, 2014, **313**, 841–849.
- 43 Q. N. Zheng, L. Wang, Y. W. Zhong, X. H. Liu, T. Chen, H. J. Yan, D. Wang, J. N. Yao and L. J. Wan, *Langmuir*, 2014, **30**, 3034–3040.
- 44 S. Lei, K. Tahara, F. C. De Schryver, M. Van der Auweraer, Y. Tobe and S. De Feyter, *Angew. Chem. Int. Edit.*, 2008, **47**, 2964–2968.
- 45 N. Thi Ngoc Ha, T. G. Gopakumar and M. Hietschold, *J. Phys. Chem. C*, 2011, **115**, 21743–21749.

- 46 L. Xu, X. R. Miao, B. Zha, K. Miao and W. L. Deng, *J. Phys. Chem. C*, 2013, **117**, 12707–12714.
- 47 L. Xu, X. R. Miao, B. Zha and W. L. Deng, *J. Phys. Chem. C*, 2012, **116**, 16014–16022.
- 5 48 M. Józefowicz and J. R. Heldt, *Chem. Phys.*, 2003, **294**, 105–116.
- 49 M. Józefowicz and J. R. Heldt, *Spectrochim. Acta, Part A*, 2007, **67**, 316–320.
- 50 M. Józefowicz, *Spectrochim. Acta, Part A*, 2007, **67**, 444–449.
- 10 51 M. Józefowicz, J. R. Heldt and J. Heldt, *Chem. Phys.*, 2006, **323**, 617–621.
- 52 T. I. Kirichenko, S. B. Meshkova, Z. M. Topilova, A. V. Kiriya, A. Y. Lyapunov, E. Y. Kulygina and N. G. Luk'yanenko, *Russ. J. Phys. Chem.*, 2005, **75**, 272–277.
- 15 53 R. Gutzler, T. Sirtl, J. r. F. Dienstmaier, K. Mahata, W. M. Heckl, M. Schmittel and M. Lackinger, *J. Am. Chem. Soc.*, 2010, **132**, 5084–5090.
- 54 A. K. Roy and A. Thakkar, *J. Chem. Phys. Lett.*, 2004, **386**, 162–168.
- 20 55 A. K. Roy and A. Thakkar, *J. Chem. Phys.*, 2005, **312**, 119–126.
- 56 G. Loveluck, *J. Phys. Chem.*, 1960, **64**, 385–387.
- 57 E. R. Mognaschi, L. Zullino and A. Chierico, *J. Phys. D- Appl. Phys.*, 1984, **17**, 1007–1012.
- 25 58 D. V. Talapin, E. V. Shevchenko, C. B. Murray, A. V. Titov and P. Král, *Nano Lett.*, 2007, **7**, 1213–1219.